

Article

Crystal Growth and the Structure of a New Quaternary Adamantine $\text{Cu}\square\text{GaGeS}_4$

Yvonne Tomm ^{1,*}, Daniel M. Többens ¹ , Galina Gurieva ¹ and Susan Schorr ^{1,2} 

¹ Helmholtz-Zentrum Berlin für Materialien und Energie, Department Structure and Dynamics of Energy Materials, Hahn-Meitner-Platz 1, 14109 Berlin, Germany

² Department Geosciences, Free University Berlin, Malteserstrasse 74-100, 12249 Berlin, Germany

* Correspondence: tomm@helmholtz-berlin.de

Abstract: Single crystals of quaternary adamantine-type $\text{Cu}\square\text{GaGeS}_4$ were grown using the chemical vapor transport technique, with iodine as the transport agent. Dark red transparent crystals were grown in a temperature gradient of $\Delta T = 900\text{--}750$ °C. Chemical characterization by X-ray fluorescence showed the off-stoichiometric composition of $\text{Cu}\square\text{GaGeS}_4$ crystals—in particular, a slight Ge deficiency was observed. By X-ray diffraction, $\text{Cu}\square\text{GaGeS}_4$ was found to adopt the chalcopyrite-type structure with the space group $I\bar{4}2d$. Cation distribution in this structure was analyzed by multiple energy anomalous synchrotron X-ray diffraction, and it was found that Cu and vacancies occupied the $4a$ site, whereas Ga and Ge occupied the $4b$ site. The band gap energies of several off-stoichiometric $\text{Cu}\square\text{GaGeS}_4$ crystals were determined by UV-Vis spectroscopy and ranged from 2.1 to 2.4 eV. A non-linear correlation of the band gap energy with the Ge content of the compound was shown to follow the usual bowing behavior of semiconductor alloys, with a bowing parameter of $b = -1.45$ (0.08).

Keywords: defect adamantine; quaternary chalcogenide; crystal growth; single crystals; structure; cation distribution; band gap energy



Citation: Tomm, Y.; Többens, D.M.; Gurieva, G.; Schorr, S. Crystal Growth and the Structure of a New Quaternary Adamantine $\text{Cu}\square\text{GaGeS}_4$. *Crystals* **2023**, *13*, 1545. <https://doi.org/10.3390/cryst13111545>

Academic Editor: Duncan H. Gregory

Received: 4 October 2023

Revised: 17 October 2023

Accepted: 23 October 2023

Published: 27 October 2023



Copyright: © 2023 by the authors. Licensee MDPI, Basel, Switzerland. This article is an open access article distributed under the terms and conditions of the Creative Commons Attribution (CC BY) license (<https://creativecommons.org/licenses/by/4.0/>).

1. Introduction

“Adamantine”-type compounds, including kesterites, are currently the most promising material for the development of a fully inorganic thin-film photovoltaic technology that is free of critical raw materials and thus provides sustainable solutions. The highest efficiency for fully inorganic thin-film photovoltaic technologies is exhibited by thin-film solar cells based on the ternary chalcopyrite-type compound semiconductor $\text{Cu}(\text{In,Ga})\text{S}_2$ (CIGS), with a record power conversion efficiency of 23.6% [1]. This absorber material belongs to the ternary $\text{A}^{\text{I}}\text{B}^{\text{III}}\text{X}^{\text{VI}}_2$ chalcopyrite-type compound, belonging to the adamantine compound family as well. One focus of research in solar energy conversion is hybrid halide perovskites, which result in thin-film devices with a record efficiency of 26.1% [1]. Despite their undisputed high efficiency, hybrid halide perovskites have some drawbacks; materials (and thus solar cell devices) have no long-term stability, and they contain lead, which is a critical toxicity issue. Furthermore, the use of Pb-containing absorber materials is not in line with the EU Directive 2002/95/EC (also known as the RoHS Directive), thereby restricting the use of lead in electrical and electronic equipment [2]. Therefore, the development of compound semiconductors that are free of critical raw materials and are long-term stable is crucial for the transition away from fossil fuels and the move toward a greener energy future. These compound semiconductors are promising materials both in single-junction solar cells and as top absorber layers in tandem cells.

The ternary $\text{A}^{\text{I}}\text{B}^{\text{III}}\text{X}^{\text{VI}}_2$ chalcopyrite compound family, which includes the compound semiconductor $\text{Cu}(\text{In,Ga})\text{Se}_2$ —used as an absorber layer in high-efficiency thin-film solar

cells—can be transformed into two different quaternary adamantines by chemical substitutions by obeying the valence octet rule. Due to added chemical and structural freedom, these quaternary compounds have some novel and exciting properties.

The first possible substitution would be $2B^{III} \leftrightarrow B^{II} + C^{IV}$, resulting in quaternary compound semiconductors $A^I_2B^{II}C^{IV}X^{VI}_4$. Such materials have recently attracted considerable attention because of their potential low costs and high-efficiency solar cell absorbers. Thin-film solar cells based on kesterite-type $Cu_2ZnSn(S,Se)_4$ (CZTSSe) not only show a record power conversion efficiency of 14.9% [1] but also show excellent long-term stability and do not contain toxic or critical components. Due to these advantages, kesterite-based thin-film solar cells are currently the only critical raw material-free and the most promising fully inorganic photovoltaic technologies. Cation alloying for band gap engineering and the extrinsic doping of kesterites to increase the power conversion efficiency of related devices have been performed by several groups. Alloying CZTSe with Ge generates solar cells with an efficiency of 12.3% [3] and alloying CZTSSe with Ag pushes the device's efficiency to 12.96% [4]. In these Ag-alloyed kesterites, mixed crystals adopt a stannite-type structure, completely blocking Cu/Zn disorder [5]—a possible reason for high V_{OC} deficits in CZTSSe-based devices. Extrinsic doping with alkali metals has been successfully used in chalcopyrite-type CIGS to achieve high energy-conversion efficiencies [6]. This approach has also been successfully adopted for kesterites. Extrinsic doping with Li can also shift the efficiency of CZTSSe to above 10% [7].

The second possible substitution would be $A^I + B^{III} \leftrightarrow C^{IV} + \square$, resulting in quaternary semiconductors $A^I\square B^{III}C^{IV}X^{VI}_4$ (the symbol \square indicates cation vacancies, i.e., empty cation sites in the crystal structure). These compounds are referred to as defect adamantines [8] and can be considered potential absorber materials for thin-film solar cell applications. However, studies on defect adamantines have made little progress since the first report by Pamplin [8]. Only a few studies on defect adamantine selenides have been published [9–11], but less information is available on sulfides [12,13]. Currently, this class of material is undergoing a renaissance because of its potential use in photovoltaic applications. For example, two studies on electronic structures and optical properties of defect adamantines have been performed by Shen et al. [14,15]. These investigations, using first-principle calculations, showed that the values of band gap energies of $Cu\square GaSnSe_4$ and $Cu\square GaGeSe_4$ were suitable for photovoltaic applications. Experimental studies on $Cu\square GaGeSe_4$ thin films [16] have shown that these compounds can be successfully used as absorber layers in thin-film solar cells. Additionally, non-linear optical parameters, such as the non-linear refractive index, have been determined [16]. Thin-film solar cells based on a $Cu\square InGeSe_4$ absorber showed a power conversion efficiency of 2.38% [17]. The crystal structure of the defect adamantine $Cu\square AlGeSe_4$ was studied by Quintero et al. [18].

In general, little is known about sulfide adamantines. In this work, a detailed study of the structural and optoelectronic properties of $Cu\square GaGeS_4$ was performed by preparing single crystals as representative materials.

1.1. Structural Considerations

Adamantines crystallize in tetrahedrally coordinated structures and were derived from diamond-type (space group $Fd\bar{3}m$) and lonsdaleite-type (space group $P\frac{6_3}{m}mc$) crystal structures. Pamplin [8] summarized 249 adamantines derived from these two different crystal structures of carbon (diamond and lonsdaleite). A pre-requisite is not only the tetrahedral coordination of cations by anions and vice versa, but also that four electrons exist per structural site and that the number of cations and anions is equal. In the case where a structural site is a vacancy, such as in $A^I\square B^{III}C^{IV}X^{VI}_4$ compounds, the compounds are referred to as “defect adamantine”.

Ternary compounds of the adamantine family, with general formula $A^I B^{III} X^{VI}_2$, crystallize in the chalcopyrite-type crystal structure (space group $I\bar{4}2d$) and belong to the tetragonal crystal system. In this crystal structure, each metal ion is tetrahedrally coordinated with four chalcogen anions and vice versa. Each anion is bonded to two mono-valent

and two three-valent cations (Figure 1). In the chalcopyrite-type crystal structure, the A^I cation occupies the Wyckoff position $4a$ at $(0, 0, 0)$, and the B^{III} cation occupies the $4b$ position at $(0, 0, 0.5)$. The anions occupy the Wyckoff position $8d$ at $(x, 0.25, 0.125)$.

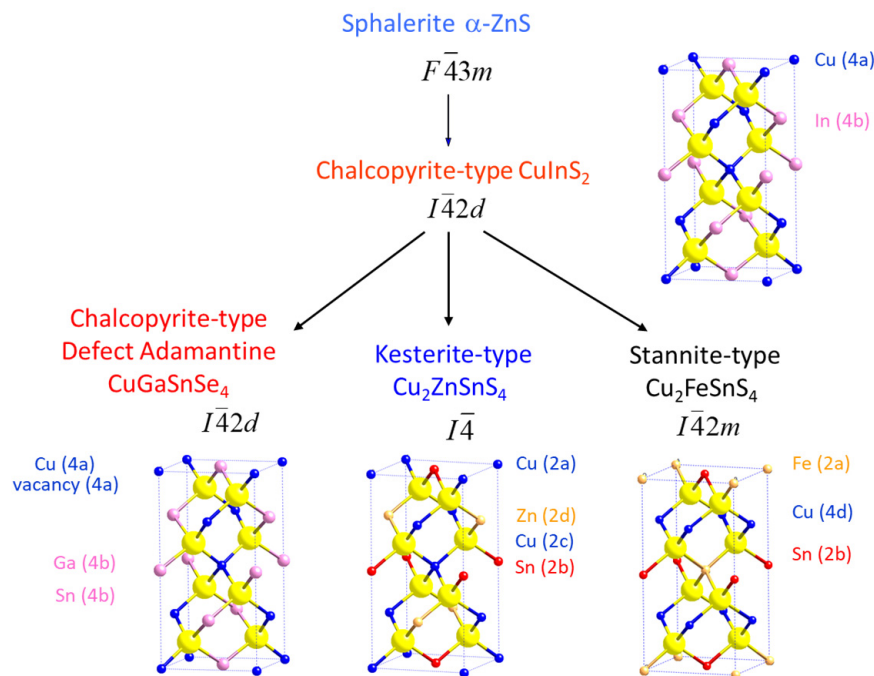


Figure 1. Adamantines—transition from tetragonal chalcopyrite-type compounds (like CuInS_2) to quaternary chalcogenides. The arrangement of cations and anions is shown, along with the resulting crystal structure type and exemplarily compounds.

Quaternary compounds of the adamantine family are of $A^I_2B^{III}C^{IV}X^{VI}_4$ and $A^I\Box B^{III}C^{IV}X^{VI}_4$ types. Figure 1 shows that the distribution of metal ions is important and determines the crystal structure of the quaternary compound. $A^I\Box B^{III}C^{IV}X^{VI}_4$ defect adamantines are formed from ternary chalcopyrite-type compounds by doubling the entire formula unit ($A^IB^{III}X^{VI}_2$) and replacing one A^{1+} and one B^{3+} cation with one C^{4+} cation. This results in a balanced valence but an unbalanced cation–anion ratio (with respect to the ratio of cation and anion sites in the chalcopyrite-type structure). Accordingly, the structure must be compensated by vacancies ($A^I + B^{III} \leftrightarrow \text{vacancy} + C^{IV}$).

1.2. Thermodynamic Properties

Limited information is available on the properties of adamantine compounds of interest. Table 1 shows structural information and the melting points and band gap energies of $\text{Cu}\Box\text{GaGeX}^{VI}_4$ with $X = \text{S, Se}$.

Table 1. Material properties of the defect adamantines $\text{Cu}\Box\text{GaGeS}_4$ and $\text{Cu}\Box\text{GaGeSe}_4$.

	$\text{Cu}\Box\text{GaGeS}_4$		$\text{Cu}\Box\text{GaGeSe}_4$	
	tetragonal [13]	tetragonal $I\bar{4}2d$ [19]	tetragonal $I\bar{4}2d$ [20]	tetragonal $I\bar{4}2d$ [21]
a (Å)	5.334	5.302	5.568	5.5617
c (Å)	10.050	10.212	10.841	10.9238
T_{melting} (°C)	1000 [9]		1000 [22]	836 [9]
$T_{\text{decomposition}}$ (°C)			710 [22]	
E_g (eV)	2.73 [23]		1.85 [20]	1.38 [10]

Little is known about the phase diagram of $\text{CuGaS}_2\text{-GeS}_2$. The phase diagram of $\text{Cu}_2\text{GeSe}_3\text{-Ga}_2\text{GeSe}_5$ [24] is used as a reference point for material synthesis (Figure 2). Very complex phase relations in the class of adamantine are obvious here. The presence of peritectic and eutectic points and phase transitions results in rather difficult conditions for single crystal growth.

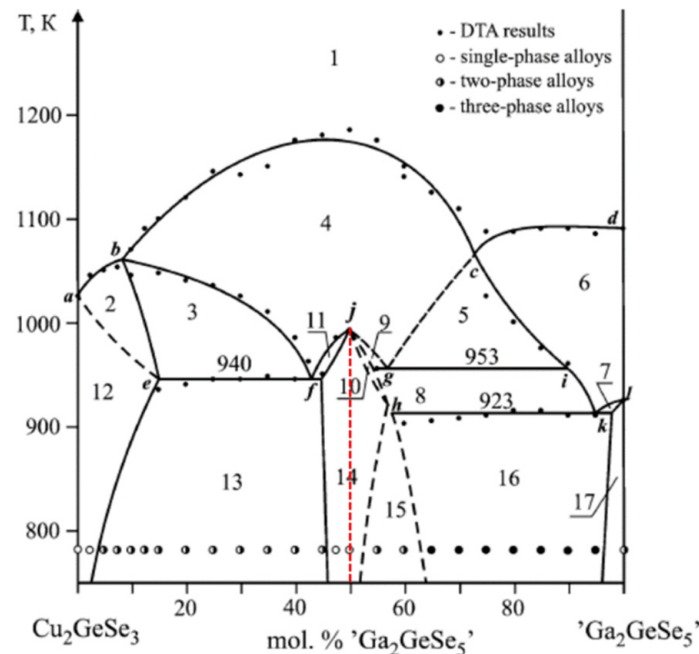


Figure 2. Phase diagram of $\text{Cu}_2\text{GeSe}_3\text{-Ga}_2\text{GeSe}_5$, adapted with permission from Strok et al. Ref. [24]. Copyright 2022, Springer Nature. The red line highlights compound $\text{Cu}\square\text{GaGeSe}_4$. Vertical section of $\text{Cu}_2\text{GeSe}_3\text{-Ga}_2\text{GeSe}_5$ (1—L, 2—L + σ , 3—L + σ + β , 4—L + β , 5—L + β + ϵ , 6—L + ϵ , 7—L + ϵ + ζ , 8—L + η + ϵ , 9—L + β + η , 10— β + η , 11—L + β + η , 12— σ , 13— σ + η , 14— η , 15— η + ϵ , 16— η + ϵ + ζ , 17— ϵ + ζ).

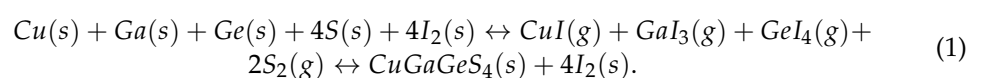
The most appropriate single crystal growth method is chemical vapor transport (as introduced by Schäfer [25] and Nitsche [26]). With chemical vapor transport (CVT) enhanced by halogens, crystals can be grown below critical temperatures. Such crystals will grow close to thermodynamic equilibrium.

In this study, we report the growth of $\text{Cu}\square\text{GaGeSe}_4$ single crystals using the chemical vapor transport technique. Starting with ternary compound CuGaS_2 , conditions for growing the single crystals of $\text{Cu}\square\text{GaGeSe}_4$ are investigated. The evolved material and crystals are characterized with respect to chemical composition, crystal structure, and band gap energy.

2. Materials and Methods

2.1. Crystal Growth

Crystal growth experiments were performed using the chemical vapor transport technique (CVT). The starting elements Cu, Ga, Ge, and S were weighed into a glassy carbon boat, which was placed in a quartz glass ampoule of 28 mm diameter and 200 mm length. A halogen element, such as iodine, was used to enhance transport. The ampoule was evacuated, closed, and placed in a two-zone furnace. The iodine reacted with metals at elevated temperatures to form volatile species. Halogen-containing species were then transported from the hot (900 °C) to the cold (750 °C) part of the ampoule. Transport occurred based on the reaction in Equation (1).



After cooling to ambient temperatures, ampoules were opened, and gaseous species present in the ampoule were allowed to evaporate.

In chemical vapor transport, growth conditions such as the temperature of the source, temperature gradient, and the concentration of the transport agent are of great importance for crystal growth. All formed phases were analyzed. The results of growth experiments—in this case, occurring phases—showed how important the consideration of the gaseous phase was for transport in a closed system. The main challenge here was to control the composition of the gas phase and optimize the temperature field during growth.

For the growth of CuGaGeS₄ crystals, most conditions were the same for all experiments; only the concentration of the transport agent iodine varied (see Table 2). The exact weights of metals and sulfur were calculated for 5 g of stoichiometric material. A temperature gradient of $\Delta T = 900\text{ }^{\circ}\text{C} - 750\text{ }^{\circ}\text{C}$ was maintained for 240 h of growth times.

2.2. Chemical Characterization

Wavelength dispersive X-ray spectroscopy (WDX) was used to determine the composition of present phases; an electron microprobe analysis system was used. In order to obtain reliable results from WDX measurements, the microprobe system was calibrated using NIST elemental standards. A high accuracy of compositional parameters was achieved by averaging over 10 local measured points within one grain and averaging over more than 30 grains of the quaternary phase showing the same compositional values.

Additionally, composition was measured by X-ray fluorescence (XRF) using a Bruker M4 Tornado Micro-XRF spectrometer with Rh excitation beams and two detectors.

2.3. Structural Characterization

X-ray diffraction: Grown crystals were characterized by powder X-ray diffraction (XRD). X-ray powder diffraction data were recorded over a 2θ range of $10\text{--}140^{\circ}$ with a step size of 0.01313° by means of a BRUKER D8 diffractometer using Cu $K\alpha_{1,2}$ radiation at wavelengths of 1.540598 \AA and 1.544426 \AA , respectively. Lattice parameters of the material were determined via a LeBail analysis of the diffraction pattern.

Multiple Edge Anomalous Diffraction (MEAD): To clarify cation distribution, anomalous X-ray powder diffraction data (AXRPD) from Cu□GaGeS₄ were collected at the KMC-2 Diffraction station at the KMC-2 beamline, BESSY II, Berlin, Germany [27], and analyzed as described in the literature [28]. Intensity scans of the 101 Bragg peak in Multiple Edge Anomalous Diffraction (MEAD) analysis were collected at the K X-ray absorption edges of the elements Cu, Ga, and Ge. Experimental absorption edges were observed at energies of $8987(1)\text{ eV}$, $10,370(1)\text{ eV}$, and $11,104(1)\text{ eV}$. These values did not deviate significantly from the literature values of 8979 eV (Cu-K), $10,367\text{ eV}$ (Ga-K), and $11,103\text{ eV}$ (Ge-K) [29], with the notable exception of the Cu-K edge, which was 8 eV higher than the reference value. Absorption corrections for experimental data were calculated based on the chemical composition of the sample, as determined experimentally by WDX. Full powder diffraction sets within the 2θ -range of $6\text{--}132^{\circ}$ were collected at energies of 8048 eV ($\lambda = 1.5406\text{ \AA}$, equivalent to Cu $K\alpha_1$) and below the absorption edges at 8965 eV , $10,353\text{ eV}$, and $11,089\text{ eV}$.

2.4. Optical Characterization

Diffuse Reflectance Spectroscopy (DRS) measurements were carried out in the air and at room temperature using a spectrophotometer equipped with an integrating sphere (Perkin Elmer UV/Vis-spectrometer Lambda 750S). The wavelength range of the measurement was adjusted to $800\text{--}1800\text{ nm}$ with a step size of 1 nm . Tauc plots were obtained by plotting $(F(R) \cdot h\nu)^2$ versus photon energies [30]. The linear part of the curve was extrapolated relative to the baseline, and the optical band gap was extracted from the value of the intersection.

Table 2. Chemical composition of off-stoichiometric $\text{Cu}_{1-x}\text{GaGeS}_4$ crystals determined by X-Ray fluorescence analysis and cation ratios. Iodine concentrations were used for crystal growth. Lattice parameters of crystals were determined using the LeBail analysis of X-ray diffraction data.

Sample No.	Chemical Formular	Cu/(Ga+Ge)	Ge/(Ga+Ge)	Iodine Concentration (mg/cm ³)	a (Å)	c (Å)	V (Å ³)
To589	$\text{Cu}_{0.93}\square_{1.08}\text{Ga}_{0.86}\text{Ge}_{1.13}\text{S}_4$	0.467	0.568	0 *	5.330(1)	10.203(2)	289.856
To557	$\text{Cu}_{1.10}\square_{0.90}\text{Ga}_{1.09}\text{Ge}_{0.91}\text{S}_4$	0.550	0.455	4.9	5.315(1)	10.114(2)	285.713
To569	$\text{Cu}_{1.18}\square_{0.83}\text{Ga}_{1.15}\text{Ge}_{0.84}\text{S}_4$	0.593	0.422	5.0	5.324(1)	10.187(2)	288.750
To585w	$\text{Cu}_{1.22}\square_{0.78}\text{Ga}_{1.25}\text{Ge}_{0.77}\text{S}_4$	0.604	0.381	8.1	5.324(1)	10.184(2)	288.265
To597	$\text{Cu}_{1.27}\square_{0.74}\text{Ga}_{1.24}\text{Ge}_{0.75}\text{S}_4$	0.638	0.377	4.7	5.319(1)	10.189(2)	287.308
To555	$\text{Cu}_{1.27}\square_{0.75}\text{Ga}_{1.22}\text{Ge}_{0.76}\text{S}_4$	0.641	0.384	4.9	5.318(1)	10.159(2)	287.845
To329	$\text{Cu}_{1.27}\square_{0.75}\text{Ga}_{1.20}\text{Ge}_{0.78}\text{S}_4$	0.641	0.394	5.0	5.318(1)	10.178(2)	287.524
To556	$\text{Cu}_{1.30}\square_{0.69}\text{Ga}_{1.24}\text{Ge}_{0.77}\text{S}_4$	0.647	0.383	4.9	5.320(1)	10.159(2)	287.650
To581	$\text{Cu}_{1.29}\square_{0.72}\text{Ga}_{1.23}\text{Ge}_{0.76}\text{S}_4$	0.648	0.382	5.0	5.323(1)	10.152(2)	288.665
To585	$\text{Cu}_{1.30}\square_{0.72}\text{Ga}_{1.23}\text{Ge}_{0.75}\text{S}_4$	0.656	0.379	8.1	5.324(1)	10.184(2)	287.642
To583	$\text{Cu}_{1.30}\square_{0.72}\text{Ga}_{1.22}\text{Ge}_{0.76}\text{S}_4$	0.657	0.384	5.0	5.319(1)	10.167(2)	286.942
To531	$\text{Cu}_{1.33}\square_{0.68}\text{Ga}_{1.27}\text{Ge}_{0.72}\text{S}_4$	0.668	0.362	5.0	5.323(1)	10.127(2)	289.856
To591	$\text{Cu}_{1.35}\square_{0.67}\text{Ga}_{1.29}\text{Ge}_{0.69}\text{S}_4$	0.682	0.348	1.1	5.324(1)	10.226(2)	291.816
To599	$\text{Cu}_{1.35}\square_{0.68}\text{Ga}_{1.24}\text{Ge}_{0.73}\text{S}_4$	0.685	0.371	3.1	5.330(1)	10.272(2)	292.484
To580	$\text{Cu}_{1.36}\square_{0.66}\text{Ga}_{1.28}\text{Ge}_{0.70}\text{S}_4$	0.687	0.353	5.0	5.362(1)	10.173(2)	291.816
To596	$\text{Cu}_{1.47}\square_{0.54}\text{Ga}_{1.42}\text{Ge}_{0.57}\text{S}_4$	0.739	0.286	4.7	5.330(1)	10.272(2)	288.665
To588	$\text{Cu}_{1.76}\square_{0.27}\text{Ga}_{1.63}\text{Ge}_{0.34}\text{S}_4$	0.893	0.173	1.1	5.340(1)	10.365(9)	295.564
literature							
	CuGaS_2 [31]	0.991	0		5.355(1)	10.485(2)	300.668
	CuGaS_2 [31]	0.995	0		5.356(1)	10.483(2)	300.723
	GeS_2 [32]	0	1		5.68	8.97	287.781

* Solid state reaction without iodine.

3. Results and Discussion

3.1. Crystal Growth

In CVT growth experiments, single crystals of $\text{Cu}_{1-x}\text{GaGeS}_4$ up to 10 mm in length were obtained, as shown in Figure 3. Crystalline materials had a dark red and orange color. In growth experiments, in addition to transparent red-orange $\text{Cu}_{1-x}\text{GaGeS}_4$ crystals, other phases also appeared, such as GeS_2 and GaI_3 .

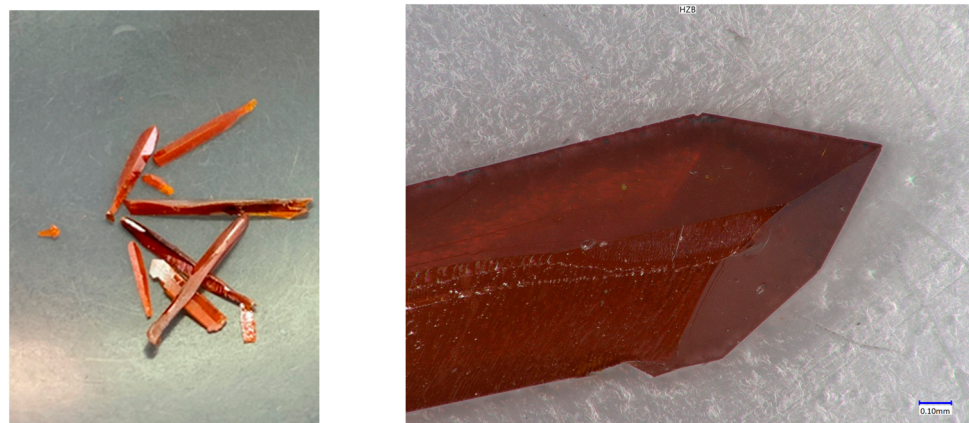


Figure 3. As-grown crystals of $\text{Cu}_{1-x}\text{GaGeS}_4$; chemical vapor transport using iodine (5 mg/cm³) as the transport agent, with $\Delta T = 900\text{ }^\circ\text{C} - 750\text{ }^\circ\text{C}$.

3.2. Chemical Composition and Off-Stoichiometry Relations

In analyzing the chemical composition of defect adamantine, chemical analysis of grown crystals by X-ray fluorescence (XRF) revealed that crystals showed Cu/(Ga+Ge) ratios between 0.45 and 0.9 and Ge/(Ga+Ge) ratios between 0.15 and 0.6 (see Table 2). Thus, single crystals showed quite a strong deviation from the stoichiometric composition, which was in accordance with $\text{Cu}/(\text{Ga}+\text{Ge}) = \text{Ge}/(\text{Ga}+\text{Ge}) = 0.5$. Therefore, defect adamantine $\text{Cu}\square\text{GaGeS}_4$ was seen as a compound that was formed within the solid solution between CuGaS_2 and GeS_2 , which can be described by $(\text{CuGaS}_2)_{1-x}(\text{GeS}_2)_x$ (see Figure 4). The general $\text{Cu}_{2(1-x)}\square_{2(1-x)}\text{Ga}_{2(1-x)}\text{Ge}_{2x}\text{S}_4$ formula can be applied to describe the off-stoichiometric composition of the material, $x = 0.5$, resulting in the stoichiometric $\text{Cu}\square\text{GaGeS}_4$ composition.

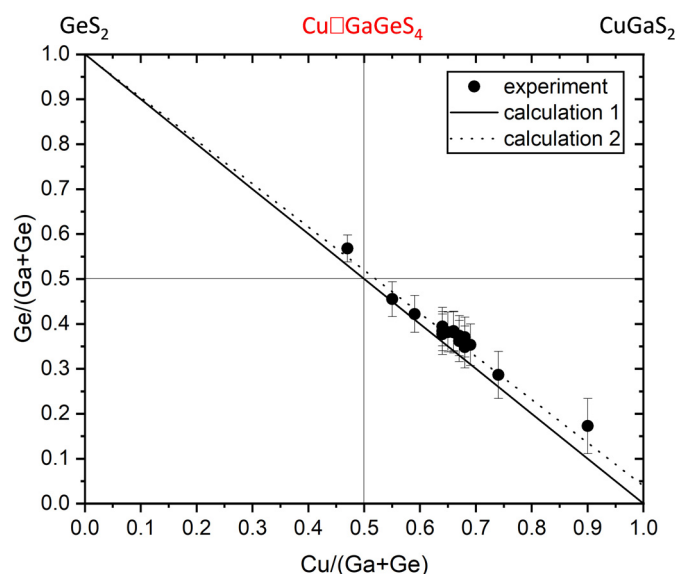


Figure 4. Experimentally determined chemical composition of off-stoichiometric $\text{Cu}\square\text{GaGeS}_4$ crystals as indicated in a cation ratio plot: $\text{Cu}/(\text{Ga}+\text{Ge})$ vs. $\text{Ge}/(\text{Ga}+\text{Ge})$. The ideal stoichiometric composition is at $\text{Cu}/(\text{Ga}+\text{Ge}) = \text{Ge}/(\text{Ga}+\text{Ge}) = 0.5$. Calculation 1 represents the composition of $\text{Cu}_{2(1-x)}\square_{2(1-x)}\text{Ga}_{2(1-x)}\text{Ge}_{2x}\text{S}_4$ crystals assuming a stoichiometric CuGaS_2 end member. For calculation 2, an off-stoichiometric end member described by $\text{Cu}_{2y}\text{Ga}_{2(1-y)}\text{S}_{3-2y}$ with $y = 0.51$ was assumed.

According to this general formula, the chemical compositions for compounds with $x = 0$ to $x = 1$ were calculated (calculation 1 and the solid line in Figure 4). Nevertheless, it is well known that CuGaS_2 and CuGaSe_2 exhibit an off-stoichiometric composition by retaining the chalcopyrite-type crystal structure [33,34]. Thus, instead of a stoichiometric end member, off-stoichiometric $\text{Cu}_{2y}\text{Ga}_{2(1-y)}\text{S}_{3-2y}$ can be assumed. The chemical compositions for compounds from $x = 0$ to $x = 1$, assuming an off-stoichiometric end member with $y = 0.51$, were calculated (calculation 2 and the dotted line in Figure 4). These calculations showed that, especially within the range of high $\text{Cu}/(\text{Ga}+\text{Ge})$ values, the experimental chemical composition of $\text{Cu}\square\text{GaGeS}_4$ single crystals agreed more with calculation 2, assuming an off-stoichiometric CuGaS_2 end member.

3.3. Crystal Structure of $\text{Cu}_{2(1-x)}\square_{2(1-x)}\text{Ga}_{2(1-x)}\text{Ge}_{2x}\text{S}_4$ Defect Adamantines

The crystal structure of the CuGaS_2 and GeS_2 end members of the $(\text{CuGaS}_2)_{1-x}(\text{GeS}_2)_x$ series were both based on a corner-sharing network of tetrahedra (see Figure 5). CuGaS_2 crystallizes in the chalcopyrite-type structure (space group $I\bar{4}2d$) formed by corner-sharing CuS_4 , GaS_4 , and GeS_4 tetrahedra [31]. For the network of corner-sharing GeS_4 tetrahedra forming the crystal structure of GeS_2 , tetragonal (space group $I\bar{4}2d$), orthorhombic (space group $Fdd2$), and monoclinic (space group Pc) modifications were reported [32,35]. The dif-

ference between these modifications is the degree of the distortion of the GeS_4 tetrahedron. The $(\text{CuGaS}_2)_{1-x}(\text{GeS}_2)_x$ series was realized by the substitution of $\text{Cu}^+ + \text{Ga}^{3+} \leftrightarrow \text{Ge}^{4+} + \square$; thus, with increasing Ge content in CuGaS_2 , the fraction of vacancies (\square) and thus the fraction of $\square\text{S}_4$ tetrahedra increased (see Figure 6).

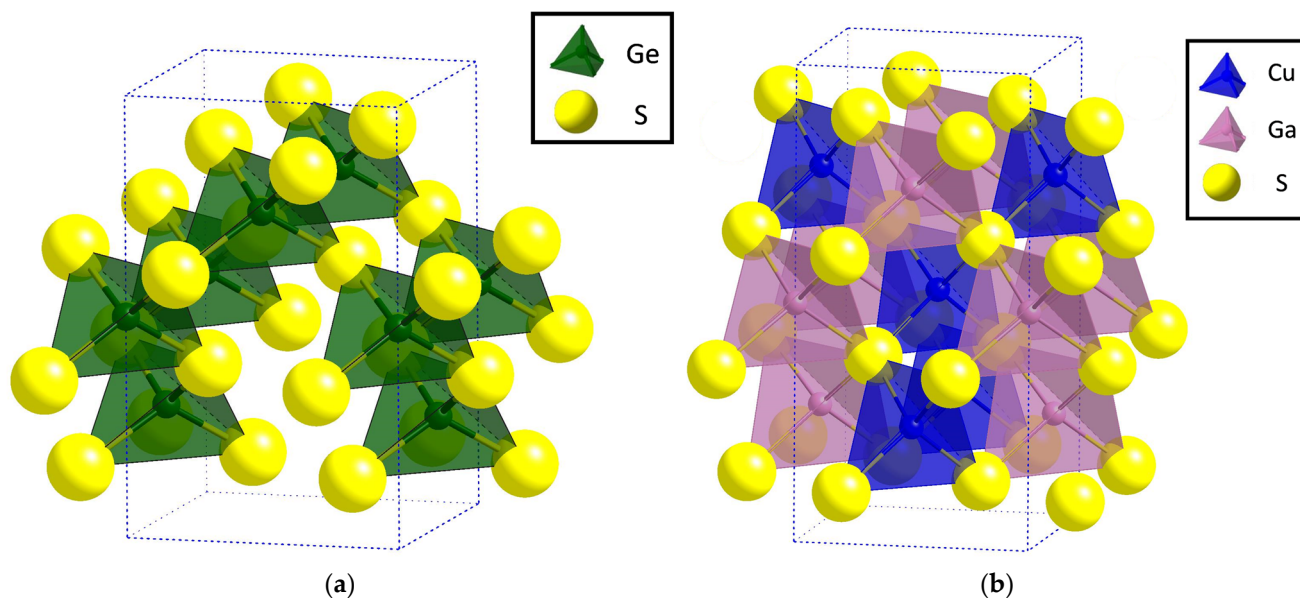


Figure 5. Crystal structure of (a) GeS_2 according to ref. [32] and (b) CuGaS_2 according to ref. [31]. CuS_4 , GaS_4 , and GeS_4 cation tetrahedra are shown. The dotted line shows the unit cell.

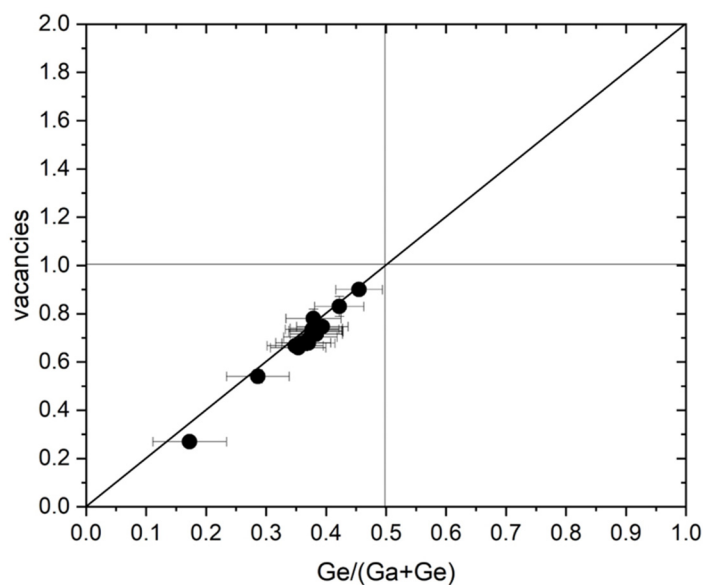


Figure 6. Fraction of vacancies in $\text{Cu}_{2(1-x)}\square_{2(1-x)}\text{Ga}_{2(1-x)}\text{Ge}_{2x}\text{S}_4$ as a dependence of Ge content. The dots show experimental values and the solid line corresponds to nominal values according to general chemical formulae above.

X-ray diffraction data on pulverized crystals were analyzed by LeBail analysis using the chalcopyrite-type structure as the structural model. An exemplarily X-ray diffractogram and corresponding LeBail analysis for a $\text{Cu}\square\text{GaGeS}_4$ single crystal (prepared as a powder) is presented in Figure 7.

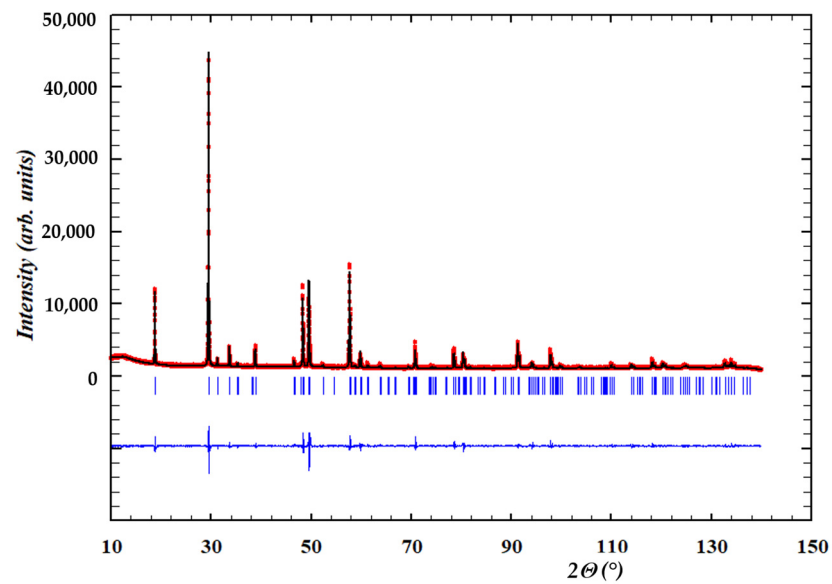


Figure 7. Example of an X-ray diffractogram of $\text{Cu}_{1.22}\square_{0.78}\text{Ga}_{1.25}\text{Ge}_{0.77}\text{S}_4$ and LeBail analysis of the data. Red dots are experimentally obtained data and blue dashes are Bragg peak positions of the chalcopyrite-type structure. The black line is the calculated fit between measured data and the structure. The blue line is the difference between experimentally obtained and calculated intensities.

Tetragonal lattice parameters a and c from different $\text{Cu}_{2(1-x)}\square_{2(1-x)}\text{Ga}_{2(1-x)}\text{Ge}_{2x}\text{S}_4$ crystals were determined by the LeBail analysis of X-ray diffraction data (see Table 2). For comparisons, the lattice constants of CuGaS_2 and GeS_2 from the literature [31,32] are also provided in Table 2. The unit cell volume correlated linearly with both $\text{Cu}/(\text{Ga}+\text{Ge})$ (see Figure 8) and $\text{Ge}/(\text{Ga}+\text{Ge})$ ratios. With increasing $\text{Cu}^+ + \text{Ga}^{3+} \leftrightarrow \text{Ge}^{4+} + \square$ substitutions in CuGaS_2 , the fraction of vacancies increased (Figure 6). In addition, the radius of the incorporated Ge^{4+} was smaller than the radius of Cu^+ and Ga^{3+} ($r_{\text{Cu}^{1+}} = 0.60 \text{ \AA}$; $r_{\text{Ga}^{3+}} = 0.47 \text{ \AA}$; $r_{\text{Ge}^{4+}} = 0.39 \text{ \AA}$ [36]). Thus, the unit cell volume decreased with increasing substitutions.

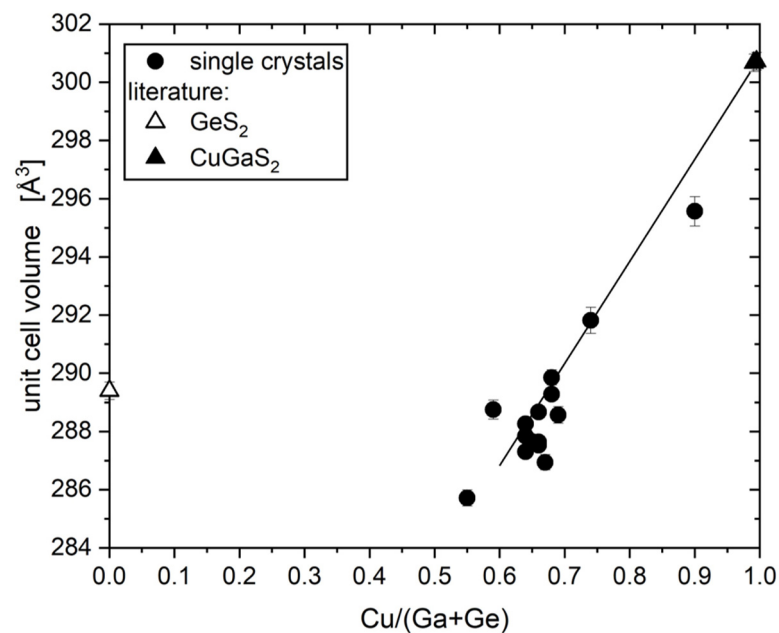


Figure 8. Unit cell volume of off-stoichiometric $\text{Cu}\square\text{GaGeS}_4$ crystals calculated from the lattice parameter as determined by LeBail analysis of XRD data as a dependence of the $\text{Cu}/(\text{Ga}+\text{Ge})$ ratio. The line should guide the eye.

With increasing $\text{Cu}^+ + \text{Ga}^{3+} \leftrightarrow \text{Ge}^{4+} + \square$ substitutions in CuGaS_2 , lattice parameters a and c changed in an anisotropic fashion; i.e., the slope of their dependence on cation ratios $\text{Cu}/(\text{Ga}+\text{Ge})$ and $\text{Ge}/(\text{Ga}+\text{Ge})$ was different (see Figure 9).

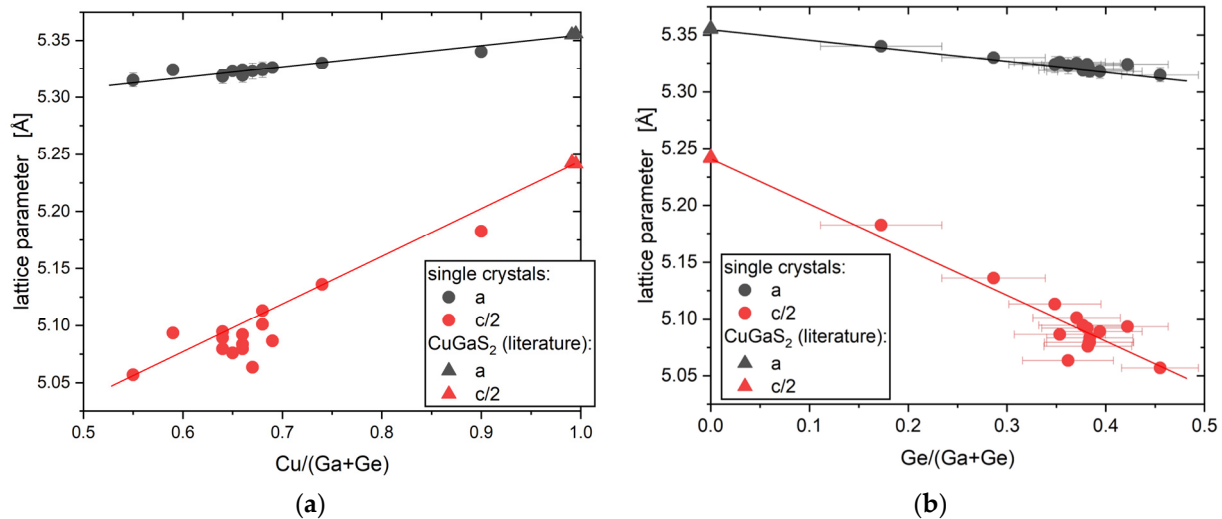


Figure 9. Correlation between lattice parameter a and the $c/2$ of off-stoichiometric $\text{Cu}\square\text{GaGeS}_4$ crystals with cation ratios (a) $\text{Cu}/(\text{Ga}+\text{Ge})$ and (b) $\text{Ge}/(\text{Ga}+\text{Ge})$. The solid lines should guide the eye.

The chalcopyrite-type structure (space group $\bar{1}42d$) had two different cation sites, Wyckoff positions $4a$ and $4b$ (Figure 10), whereas the mono-valent cation occupied the $4a$ position, and the three-valent cation occupied the $4b$ position. As Cu^+ , Ga^{3+} , and Ge^{4+} had the same number of electrons, their X-ray atomic form factors were very similar. Thus, the determination of cation distribution on the two structural sites of the chalcopyrite-type structure by conventional X-ray diffraction was not possible. Published results on the crystal structure of $\text{Cu}\square\text{GaGeSe}_4$, which were based on investigations by X-ray diffraction, assumed either Cu and vacancies on $4a$ and Ga and Ge on $4b$ positions [20] or Cu and Ga on $4a$ and Ge and vacancies on $4b$ sites [21] (see Figure 10). However, it was also possible for Cu and Ge to occupy $4b$, in addition to various degrees of cation disorder.

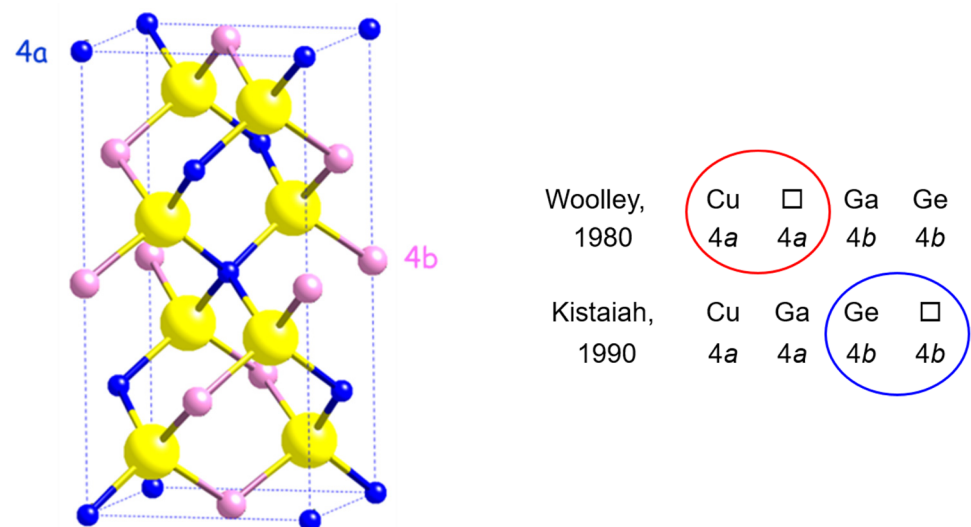


Figure 10. Chalcopyrite-type structure and cation and vacancy distributions according to Woolley [20] and Kistaiah [21].

Multiple Edge Anomalous Diffraction (MEAD) using synchrotron X-rays is an established experimental method that distinguishes electronically similar elements during data analysis [28]. The experimental MEAD spectrum was compared to calculated spectra (see Figure 11). As a structural model in calculated spectra, the chalcopyrite-type structure was used, but it was used with three different cation distributions. For calculations, the structural parameters for $\text{Cu}\square\text{GaGeSe}_4$ (from Woolley [20]) and the ideal stoichiometric composition were assumed. In addition, a calculated spectrum based on the final refined crystal structure (Table 3) was also shown; differences relative to the ideal model were negligible.

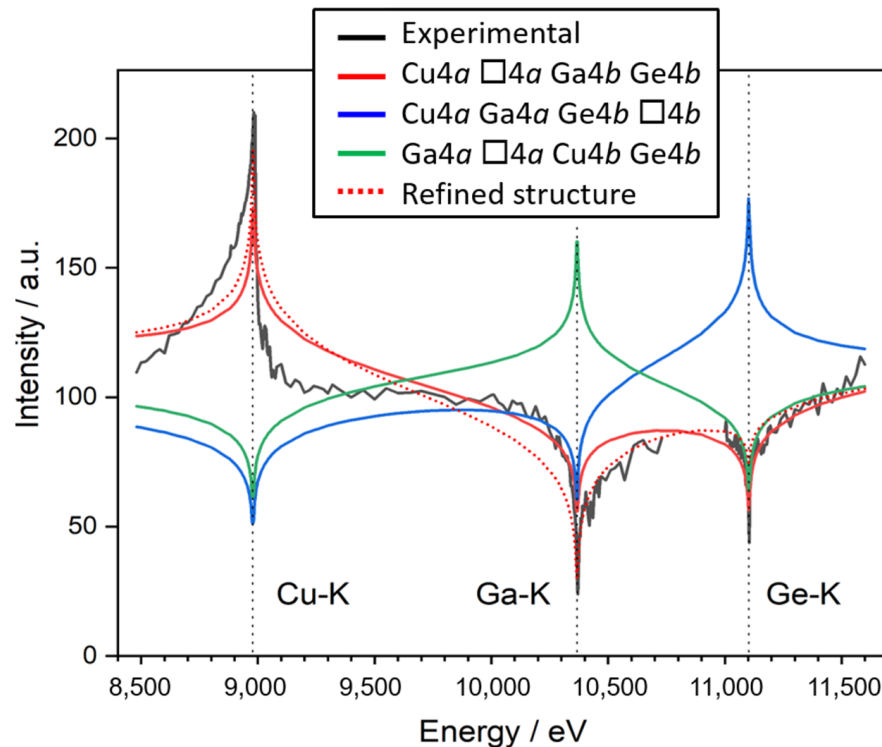


Figure 11. MEAD analysis of the energy dependency of the 101 Bragg peak intensity of $\text{Cu}_{1.22}\square_{0.78}\text{Ga}_{1.25}\text{Ge}_{0.77}\text{S}_4$. Curves are normalized relative to an average intensity of 100.

Table 3. Results showing the structural refinement of MEAD data for $\text{Cu}_{1.22}\text{Ga}_{1.25}\text{Ge}_{0.77}\text{S}_4$.

Composition (refined): $\text{Cu}_{1.152(3)} \text{Ga}_{1.554(26)} \text{Ge}_{0.446(26)} \text{S}_{3.799(13)}$						
Space group : $I\bar{4}2d$						
Atom	Wyckoff	<i>x</i>	<i>y</i>	<i>z</i>	Biso [\AA^2]	s.o.f.
Cu	4a	0	0	0	0.830(36)	0.576(2)
Ga	4b	0	0	0.5	0.909(15)	0.777(13)
Ge	4b	0	0	0.5	0.909(15)	0.223(13)
S	8d	0.25518(20)	0.25	0.125	0.804	0.950(3)
S Anisotropic	U11 = 0.010(2), U22 = 0.0029(19), U33 = 0.0179(7), U12 = 0, U13 = 0, U23 = 0.0041(7)					
Lattice parameter	$a = 5.321383(10) \text{ \AA}$		$c = 10.18642(3) \text{ \AA}$		$V = 288.4500(12) \text{ \AA}^3$	
Overall fit indicators (referring to the combined four diffraction patterns):						
$R_{\text{wp}} = 0.067$		$\text{Chi}^2 = 11.7$		$\text{Bérar SCOR [37]} = 4.42$		

It was obvious that the real cation distribution showed that Cu and vacancies occupied the $4a$ site and Ga and Ge occupied the $4b$ site.

A subsequent joint Rietveld refinement of the structure using diffraction patterns collected with four different X-ray energies confirmed this result. Due to anomalous scattering, which resulted in a change in the scattering power of chemical elements between individual datasets, the simultaneous independent refinement of all cation site occupation factors was possible. However, this resulted in rather high uncertainties, and the structural model was subsequently simplified by removing atoms with (unphysical) negative occupation factors and limiting total site occupation to full occupation. Note that this was not compulsive; interstitial cations could not be excluded by the methods presented here. The resulting model (Figure 12) was in full agreement with the results from MEAD analyses, with only copper on the $4a$ position and gallium and germanium on the $4b$ position, but not copper. Vacancies were found on $4a$ and $8d$ anion sites; the $4b$ Wyckoff site with the highest site occupation factor was assumed to be fully occupied. During the final step, charge neutrality between Cu^{1+} , Ga^{3+} , Ge^{4+} , and S^{2-} was forced; this did not result in a reduction in fit quality and did not significantly affect the refined values of site occupation factors. The results of the refinement are shown in Table 3.

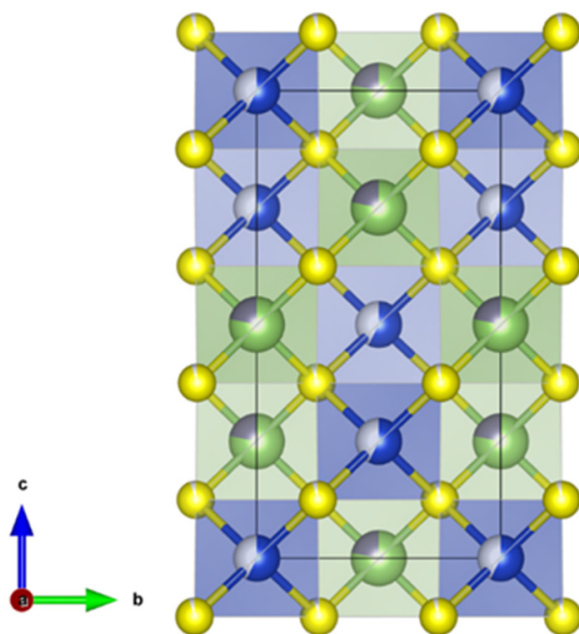


Figure 12. Refined structure of $\text{Cu}_{1.22}\square_{0.78}\text{Ga}_{1.25}\text{Ge}_{0.77}\text{S}_4$ with site occupation indicated. Cu/vacancies, blue/sky blue; Ge/Ga, green/turquoise.

3.4. Band Gap Energy

Band gap energy was determined from diffuse reflectance as measured using UV-VIS spectroscopy. Using the following Kubelka–Munk pseudo-absorption function [38,39]

$$F(R) = \frac{(1 - R)^2}{2R}, \quad (2)$$

the band gap energy E_g was determined from the linear slope of function $(F(R) \cdot h\nu)^2$, assuming a direct band gap for the material studied.

Table 4 summarizes the band gap energies of several off-stoichiometric $\text{Cu}\square\text{GaGeS}_4$ crystals and their chemical composition. A non-linear correlation was observed between chemical composition and band gap energy.

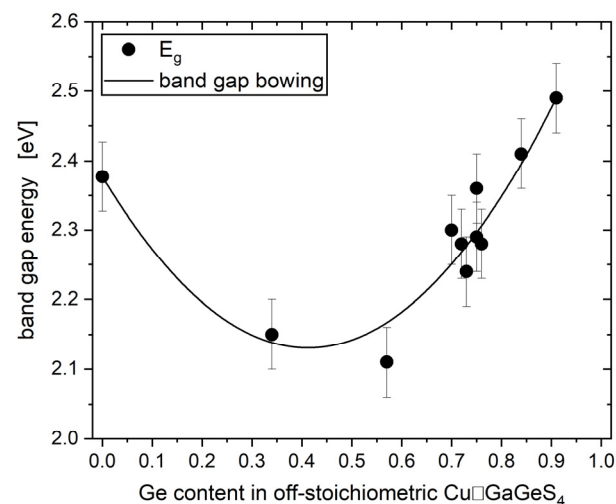
Table 4. Results for off-stoichiometric $\text{Cu}\square\text{GaGeS}_4$ crystals: chemical composition and their band gap energies as determined by UV-Vis spectroscopy.

Sample No.	Composition	Band Gap Energy E_g (eV)
To557	$\text{Cu}_{1.10}\square_{0.90}\text{Ga}_{1.09}\text{Ge}_{0.91}\text{S}_4$	2.49(5)
To569	$\text{Cu}_{1.18}\square_{0.83}\text{Ga}_{1.15}\text{Ge}_{0.84}\text{S}_4$	2.41(5)
To597	$\text{Cu}_{1.27}\square_{0.74}\text{Ga}_{1.24}\text{Ge}_{0.75}\text{S}_4$	2.29(5)
To581	$\text{Cu}_{1.29}\square_{0.72}\text{Ga}_{1.23}\text{Ge}_{0.76}\text{S}_4$	2.28(5)
To585	$\text{Cu}_{1.30}\square_{0.72}\text{Ga}_{1.23}\text{Ge}_{0.75}\text{S}_4$	2.36(5)
To531	$\text{Cu}_{1.33}\square_{0.68}\text{Ga}_{1.27}\text{Ge}_{0.72}\text{S}_4$	2.28(5)
To599	$\text{Cu}_{1.35}\square_{0.68}\text{Ga}_{1.24}\text{Ge}_{0.73}\text{S}_4$	2.24(5)
To580	$\text{Cu}_{1.36}\square_{0.66}\text{Ga}_{1.28}\text{Ge}_{0.70}\text{S}_4$	2.30(5)
To596	$\text{Cu}_{1.47}\square_{0.54}\text{Ga}_{1.42}\text{Ge}_{0.57}\text{S}_4$	2.11(5)
To588	$\text{Cu}_{1.76}\square_{0.27}\text{Ga}_{1.63}\text{Ge}_{0.34}\text{S}_4$	2.15(5)

The band gap energy of semiconductor alloys is usually described by a quadratic polynomial as a function of the concentration of an alloy component, with the quadratic coefficient referred to as the “bowing parameter”. Accordingly, the band gap energy E_g of alloy $(2\text{CuGaS}_2)_{1-x}(\text{Cu}\square\text{GaGeS}_4)_x$ is described by

$$E_g(x) = xE_g(\text{Cu}\square\text{GaGeS}_4) + (1-x)E_g(\text{CuGaS}_2) - bx(1-x). \quad (3)$$

Here, b is the bowing parameter. Figure 13 shows the experimentally determined band gap energy of $(2\text{CuGaS}_2)_{1-x}(\text{Cu}\square\text{GaGeS}_4)_x$ crystals and band gap bowing according to Equation (3). In the respective fit, Ge content of crystals was selected to represent the x value in Equation (3). The bowing parameter was determined as $b = -1.45(0.08)$ and described the deviation from linearity.

**Figure 13.** Band gap energies of different crystals within the $(2\text{CuGaS}_2)_{1-x}(\text{Cu}\square\text{GaGeS}_4)_x$ alloy. CuGaS_2 is the end member of the alloy for $x = 0$ and the right end member is represented by off-stoichiometric $\text{Cu}\square\text{GaGeS}_4$ crystal with the highest Ge content. The solid line represents the fit of experimental band gap energy values relative to Equation (3), describing the bowing behavior.

4. Conclusions

Defect adamantines are interesting and promising materials for photovoltaic applications, and are free of critical raw materials. Quaternary adamantines can be derived directly from ternary chalcopyrite $\text{A}^{\text{I}}\text{B}^{\text{III}}\text{X}^{\text{VI}}_2$. In the doubled chemical formula, one A^{1+} and one B^{3+} are replaced by one C^{4+} atom, resulting in cation vacancies containing quaternary compounds with the general formula $\text{A}^{\text{I}}\square\text{B}^{\text{III}}\text{C}^{\text{IV}}\text{X}^{\text{VI}}_4$ while maintaining tetrahedral coordination.

Cu□GaGeS₄ single crystals were grown using the chemical vapor transport technique. Their chemical composition was found to vary and deviate significantly from the stoichiometric composition. Therefore, grown crystals were described as compounds of a solid solution between CuGaS₂ and GeS₂, forming (CuGaS₂)_{1-x}(GeS₂)_x alloys. The Cu/(Ga+Ge) and Ge/(Ga+Ge) cation ratios described the deviation from the stoichiometric composition (Cu/(Ga+Ge) = Ge/(Ga+Ge) = 0.5). Structural and optoelectronic properties were considerably influenced by these cation ratios and the number of vacancies.

It was shown that Cu□GaGeS₄ crystallized in the chalcopyrite-type structure (space group $\bar{I}42d$). The cation distribution in this structure, analyzed using MEAD, was determined to be Cu and vacancies on the Wyckoff position 4a and Ga and Ge were observed on Wyckoff position 4b of the chalcopyrite-type structure.

The band gap energy E_g of off-stoichiometric Cu□GaGeS₄ crystals varied between 2.1 and 2.4 eV. The non-linear correlation between band gap energy E_g and the chemical composition (Ge content) was described by the usual bowing behavior of semiconductor alloys, with a bowing parameter of $b = -1.45(0.08)$.

Author Contributions: The manuscript was written with the contribution of all authors. Conceptualization, Y.T. and S.S.; methodology, Y.T., G.G., D.M.T. and S.S.; validation, Y.T., G.G., D.M.T. and S.S.; formal analysis, Y.T., G.G. and D.M.T.; investigation, Y.T., G.G., D.M.T. and S.S.; data curation, Y.T.; writing—original draft preparation, Y.T. and S.S.; writing—review and editing, Y.T., G.G., D.M.T. and S.S.; visualization, Y.T., G.G., D.M.T. and S.S.; supervision, S.S. All authors have read and agreed to the published version of the manuscript.

Funding: This research received no external funding.

Data Availability Statement: Data can be provided by the corresponding author by request.

Acknowledgments: AXRPD measurements were carried out using the diffraction instrument at the KMC-2 beamline at Helmholtz-Zentrum Berlin für Materialien und Energie GmbH, Berlin, Germany. We thank HZB for the allocation of synchrotron radiation beamtimes.

Conflicts of Interest: The authors declare no conflict of interest.

References

1. Best Research-Cell Efficiency Chart, NREL. Available online: <https://www.nrel.gov/pv/cell-efficiency.html> (accessed on 14 October 2023).
2. EUR-Lex.europa. Available online: <http://data.europa.eu/eli/dir/2011/65/2016-07-15> (accessed on 14 October 2023).
3. Kim, S.; Kim, K.M.; Tampo, H.; Shibata, H.; Niki, S. Improvement of voltage deficit of Ge-incorporated kesterite solar cells with 12.3% conversion efficiency. *Appl. Phys Express* **2016**, *9*, 102301. [[CrossRef](#)]
4. Gong, Y.; Zhu, Q.; Li, B.; Wang, S.; Duan, B.; Lou, L.; Xiang, C.; Jedlicka, E.; Giridharagopal, R.; Zhou, Y.; et al. Elemental de-mixing-induced epitaxial/CdS interface enabling 13% efficiency solar cells. *Nat. Energy* **2022**, *7*, 966–997. [[CrossRef](#)]
5. Gurieva, G.; Marquez, J.A.; Franz, A.; Hages, C.J.; Levenco, S.; Unold, T.; Schorr, S. Effect of Ag incorporation on structure and optoelectronic properties of (Ag_{1-x}Cu_x)₂ZnSnSe₄ solid solutions. *Phys. Rev. Mater.* **2020**, *4*, 054602. [[CrossRef](#)]
6. Wang, Y.; Lv, S.; Li, Z. Review of incorporation of alkali elements and their effects in Cu(In,Ga)Se₂ solar cells. *J. Mater. Sci. Technol.* **2022**, *96*, 179–189. [[CrossRef](#)]
7. Giraldo, S.; Jehl, Z.; Placidi, M.; Izquierdo-Roca, V.; Perez-Rodriguez, A.; Saucedo, E. Progress and Perspectives of Thin Film Kesterite Photovoltaic Technology: A Critical Review. *Adv. Mater.* **2019**, *31*, 1806692. [[CrossRef](#)]
8. Pamplin, B. The Adamantine Family of Compounds. *Prog. Cryst. Growth Charact.* **1981**, *3*, 179–192. [[CrossRef](#)]
9. Matsushita, H.; Katsui, A. Materials design for Cu-based quaternary compounds derived from chalcopyrite-rule. *J. Phys. Chem. Solids* **2005**, *66*, 1933–1936. [[CrossRef](#)]
10. Maeda, T.; Matsushita, H.; Katsui, A. Crystal growth of Cu-III-Ge-Se₄ Quaternary compounds (III = Ga, In) by vertical Bridgman methods. *Jpn. J. Appl. Phys.* **2000**, *39*, 41–43. [[CrossRef](#)]
11. Lopez-Rivera, S.A.; Pamplin, B.R.; Woolley, J.C. High-Temperature lattice parameters and DTA of the quaternary compound CuGaSn□Se₄. *Il Nuovo C.* **1983**, *2*, 1728–1735. [[CrossRef](#)]
12. Garbato, L.; Geddo-Lehmann, A.; Ledda, F. Growth and structural properties of quaternary copper thiostannates. *J. Cryst. Growth* **1991**, *114*, 299–306. [[CrossRef](#)]
13. Hahn, H.; Strick, G. Über quaternäre Chalkogenide zinkblendeähnlicher Struktur. *Naturwiss.* **1967**, *54*, 225–226. [[CrossRef](#)]
14. Shen, K.; Lu, H.; Zhang, X.; Jiao, Z. Numerical studies of the electronic structure, elastic and optical properties of defect quaternary semiconductor CuGaSnSe₄. *Results Phys.* **2018**, *9*, 49–54. [[CrossRef](#)]

15. Shen, K.; Zhang, X.; Lu, H.; Jiao, Z. Numerical study of the defect adamantine compound CuGaGeSe₄. *Mol. Phys.* **2018**, *116*, 1551–1557. [[CrossRef](#)]
16. Hassanien, A.S.; Almari, H.R.; El Radaf, I.M. Impact of film thickness on optical properties and optoelectrical parameters of novel CuGaGeSe₄ thin films synthesized by electron beam deposition. *Opt. Quantum Electron.* **2020**, *52*, 335. [[CrossRef](#)]
17. Hameed, T.A.; Wassel, R.A.; El Radaf, I.M.; Elsayed-Ali, H.E. Characterization of CuInGeSe₄ thin films and Al/n-Si/-CuInGeSe₄/Au heterojunction device. *J. Mater. Sci. Mater. Electron.* **2018**, *29*, 12584–12594. [[CrossRef](#)]
18. Delgado, G.E.; Quintero, M. Synthesis and structural characterization using Rietveld method of the quaternary compound CuAlGeSe₄. *Rev. Mex. Fis.* **2022**, *68*, 020501. [[CrossRef](#)]
19. Pamplin, B.R.; Ohachi, T.; Maeda, S.; Negrete, P.; Elworthy, T.P.; Sanderson, R.; Whitlow, H.J. Solubility of the group IV chalcogenides in I-III-VI₂ compounds. In *Ternary Compounds*; Holah, G.D., Ed.; Institute of Physics Publishing: Bristol, UK, 1977; pp. 35–42.
20. Woolley, J.C.; Goodchild, R.G.; Hughes, O.H.; Lopez-Rivera, S.A.; Pamplin, B.R. Quaternary Defect Chalcopyrite Compounds I III IV VI₄. *Jpn. J. Appl. Phys.* **1980**, *19* (Suppl. 19-3), 145–148. [[CrossRef](#)]
21. Kistaiah, P.; Vishnuvardhan Reddy, C.; Satyanarayana Murthy, K. Thermal-expansion anisotropy in the quaternary semiconductor CuGaGe_{1-x}(VGe)_xSe₄ at elevated temperatures. *Phys. Rev. B* **1990**, *42*, 7186–7192. [[CrossRef](#)]
22. Lopez Rivera, A. Quaternary Defect Adamantine Compounds of the Type I-III-IV-VI₂-VI₄. Doctoral Thesis, University of Bath, Bath, UK, 1981.
23. Panyutin, V.L.; Ponedelnikov, B.E.; Chizhikov, V.I. Energy band spectra of mercury selenogermanate and copper thiogermanogalate. *Sov. Phys. Semicond.* **1983**, *17*, 1061–1062.
24. Strok, O.M.; Olekseyuk, I.D.; Zmiy, O.F.; Ivashchenko, I.A.; Gulay, L.D. The Quasi-ternary system Cu₂Se-Ga₂Se₃-GeSe₂. *J. Phase Equilibria Diffus.* **2013**, *34*, 94–103. [[CrossRef](#)]
25. Schäfer, H. *Chemical Transport Reactions*; Academic Press: New York, NY, USA; London, UK, 1964.
26. Nitsche, R. Kristallzucht aus der Gasphase durch chemische Transportreaktionen. *Fortschr. Miner.* **1967**, *44*, 231–287.
27. Többens, D.M.; Zander, S. Helmholtz-Zentrum Berlin für Materialien und Energie, KMC-2: X-ray beamline with dedicated diffraction and XAS endstations at BESSY II. *J. Large-Scale Res. Facil.* **2016**, *2*, A49. [[CrossRef](#)]
28. Többens, D.M.; Gurieva, G.; Niedenzu, S.; Schuck, G.; Zizak, I.; Schorr, S. Cation distribution in Cu₂ZnSnSe₄, Cu₂FeSn₄ and Cu₂ZnSiSe₄ by multiple-edge anomalous diffraction. *Acta Cryst. B* **2020**, *B76*, 1027–1035. [[CrossRef](#)] [[PubMed](#)]
29. Merritt, E.A. *X-ray Anomalous Scattering*; Biomolecular Structure Center the University of Washington: Seattle, WA, USA, 2014.
30. Tauc, J.; Grigorovici, R.; Vanacu, A. Optical properties and electronic structure of amorphous Germanium. *Phys. Stat. Sol.* **1966**, *15*, 627–637. [[CrossRef](#)]
31. Stephan, C. Structural Trends in Off-Stoichiometric Chalcopyrite Type Compound Semiconductors. Ph.D. Thesis, Freie Universität Berlin, Berlin, Germany, 2011.
32. The Materials Project. mp-7582. Available online: <https://next-gen.materialsproject.org> (accessed on 17 July 2023).
33. Stephan, C.; Schorr, S.; Schock, H.-W. New Structural Investigations in the Cu₂Se(S)-In₂Se₃(S)/Cu₂Se(S)-Ga₂Se₃(S) Phase Diagrams. In *Thin-Film Compound Semiconductor Photovoltaics—2009*; Yamada, A., Heske, C., Contreras, M., Igalson, M., Irvine, S.J.C., Eds.; Materials Research Society Symposium Proceedings; Cambridge University Press: Cambridge, UK, 2009; 1165-M09-08.
34. Stephan, C.; Scherb, T.; Kaufmann, C.; Schorr, S.; Schock, H.-W. Cationic point defects in CuGaSe₂ from a structural perspective. *Appl. Phys. Lett.* **2012**, *101*, 101907. [[CrossRef](#)]
35. Dittmar, G.; Schäfer, H. Die Kristallstruktur von L.T.-GeS₂. *Acta Crystallogr.* **1976**, *B32*, 1188–1192. [[CrossRef](#)]
36. Shannon, R.D. Revised effective ionic radii and systematic studies of interatomic distances in halides and chalcogenides. *Acta Cryst. A* **1976**, *32*, 751–767. [[CrossRef](#)]
37. Bézar, J.-F.; Lelann, P. E.S.D.'s and estimated probable error obtained in Rietveld refinements with local correlations. *J. Appl. Cryst.* **1991**, *24*, 1–5. [[CrossRef](#)]
38. Kubelka, P.; Munk, F. Ein Beitrag zur Optik der Farbanstriche. *Z. Technol. Phys.* **1931**, *12*, 593–601.
39. Kubelka, P. New contributions to the optics of intensely light-scattering materials. Part I. *J. Opt. Soc. Am.* **1948**, *38*, 448–457. [[CrossRef](#)]

Disclaimer/Publisher's Note: The statements, opinions and data contained in all publications are solely those of the individual author(s) and contributor(s) and not of MDPI and/or the editor(s). MDPI and/or the editor(s) disclaim responsibility for any injury to people or property resulting from any ideas, methods, instructions or products referred to in the content.